 CMES, vol.26, no.3, pp.189-207, 2008

2D and 3D Boundary Element Analysis of Mode-I Cracks in Gradient Elasticity

G.F. Karlis [1], S.V. Tsinopoulos [2], D. Polyzos [3] and D.E. Beskos [4]

Abstract: A boundary element method, suitable for solving two and three dimensional gradient elastic fracture mechanics problems under static loading, is presented. A simple gradient elastic theory (a simplied version of Mindlin's Form-II general theory of gradient elasticity) is employed and the static gradient elastic fundamental solution is used to construct the boundary integral representation of the problem with the aid of a reciprocal integral identity. In addition to a boundary integral representation for the displacement, a boundary integral representation for its normal derivative is also necessary for the complete formulation of a well-posed problem. Surface quadratic line and quadrilateral boundary elements are employed for the two- and three dimensional case, respectively and the discretization is restricted only to the boundary. Two new special variable-order singularity discontinuous elements for two- and three-dimensional cases are proposed for the treatment of singular fields around the tip or the front of the crack and the numerical determination of the corresponding stress intensity factors (SIFs). Two numerical examples dealing with two- and three-dimensional mode-I cracks are presented and discussed.

Keyword: Boundary Elements, fracture, crack, mode-I, gradient elasticity.

[1] Department of Mechanical and Aeronautical Engineering, University of Patras, GR- 26500 Patras, Greece

[2] Department of Mechanical Engineering, Technological and Educational Institute of Patras, GR-26334, Patras, Greece

[3] Department of Mechanical and Aeronautical Engineering, University of Patras, GR- 26500 Patras, Greece and Institute of Chemical Engineering and High Temperature Chemical Process, GR-26504, Patras, Greece

[4] Department of Civil Engineering, University of Patras, GR-26500 Patras, Greece and Office of Theoretical and Applied Mechanics, Academy of Athens, GR-11527 Athens, Greece

1 Introduction

It is well known that in classical elasticity all the fundamental quantities and material constants defined at any point of an elastic body are taken as mean values over very small volume elements the size of which must be sufficiently large in comparison with the material microstructure. Considering a very simple example and taking Taylor expansions for displacements around the point of interest, Exadaktylos and Vardoulakis (2001) explain that this assumption is possible only when displacements are constant or vary linearly throughout the aforementioned representative volume elements. In cases where non-linear variations of displacements are observed, higher order Taylor expansion terms and thus higher order gradients of displacements should be taken into account. Making use of higher Taylor terms, however, some new internal length scale constants correlating the microscopic representative volume element with the macrostructure are introduced in the constitutive equations of the considered elastic continuum. Thus, in fracture mechanics and dislocation problems where near the tip of the crack and dislocation lines abrupt changes of strains and stresses are observed, enhanced elastic theories that take into account higher order gradients of strains and stresses and introduce new internal length scale parameters to describe microstructural effects, should be applied. Among those who have developed such theories one can mention Mindlin (1964), Mindlin (1965), Mindlin and Eshel (1968), Green and Rivlin (1964), Aifantis (1992), Ru and Aifantis (1993), Vardoulakis and Sulem (1995), Exadaktylos and Vardoulakis (1998), Fleck and Hutchinson

(1997), and Fleck and Hutchinson (2001). In the regime of isotropic linear elastic behaviour, the most general and comprehensive gradient elastic theory is the one due to Mindlin (1964). However, in order to balance the dimensions of strains and higher order gradients of strains as well as to correlate the micro-strains with macro-strains, Mindlin utilized eighteen new constants rendering thus his initial general theory very complicated from physical and mathematical point of view. For this reason, considering long wavelengths and the same deformation for macro and micro structure Mindlin proposed three new simplified versions of his theory, known as Form-I, II and III, where beyond the two Lamè constants other five ones are introduced instead of sixteen employed in his initial model. In Form-I, the strain energy density function is assumed to be a quadratic form of the classical strains and the second gradient of displacement; in Form-II the second displacement gradient is replaced by the gradient of strains and in Form-III the strain energy function is written in terms of the strain, the gradient of rotation and the fully symmetric part of the gradient of strain. The most important difference among the aforementioned three simplified versions of the general Mindlin's theory is the fact that the Form-II leads to a total stress tensor, which is symmetric as in the case of classical elasticity. This symmetry avoids the problems introduced by the non-symmetric stress tensors in Cosserat, micropolar and couple stress theories. Aifantis (1992) and Ru and Aifantis (1993) proposed a very simple gradient elastic model requiring only one new gradient elastic constant besides the standard Lamè ones. As it is mentioned in Vardoulakis, Exadaktylos, and Aifantis (1996) this gradient elastic model can be considered as the simplest possible special case of Form-II version of Mindlin's theory. Vardoulakis and Sulem (1995) proposed the gradient elastic theory with surface energy, a rigorous theory that can be considered as a direct consequence of the continuum model proposed by Casal (1972). Finally, Fleck and Hutchinson (1997) and Fleck and Hutchinson (2001) decomposed the second gradient of displacement into the stretch gradient and the rotation gradient tensors thus proposing an alternative version of Mindlin's Form-I gradient elastic theory. The aforementioned theories seem to be ideal for studying the strain and stress fields near the crack tip at the microscale. For this reason many analytical works dealing with two dimensional, gradient elastic, fracture mechanics problems under conditions of plane strain or anti-plane strain have appeared in the literature. One can mention here the analytical works of Vardoulakis, Exadaktylos, and Aifantis (1996), Exadaktylos, Vardoulakis, and Aifantis (1996), Vardoulakis and Exadaktylos (1997), Exadaktylos (1998), Huang, Zhang, Guo, and Hwang (1997), Zhang, Huang, Chen, and Hwang (1998), Shi, Huang, and Hwang (2000), Fannjiang, Chan, and Paulino (2002), Georgiadis (2003), Georgiadis and Grentzelou (2006), Tong, Lam, and Yang (2005) and Radi (2008). The main conclusion they reach is that near the crack tip displacements and strains behave as $r^{3/2}$ and $r^{1/2}$ functions, respectively, with r being the distance from the crack tip, while double stresses and total stresses exhibit a singular behaviour of order $r^{-1/2}$ and $r^{-3/2}$, respectively. The important part of these results is that gradient elastic theories predict the same cusp-like crack shape near the crack tip with Barenblatt's cohesive zone theory (Barenblatt (1962)) without demanding extra interatomic forces beyond those imposed by the non-classical boundary conditions. On the other hand, stress fields near the tip of the crack remain singular. In all these analytical works no computation of stress intensity factors (SIFs) has been reported because of the complexity of the problem. It is obvious that for complex gradient elastic fracture mechanics problems use of numerical methods of solution is imperative. The Finite Element Method (FEM) and the Boundary Element Method (BEM) are two very well-known and robust methods for solving elastic fracture mechanics problems(Nishioka, Kabayashi, and Fujimoto (2007), Fujimoto and Nishioka (2006), Shah, Tan, and Wang (2006), Zhang and Savaidis (2003) and Wen, Aliabadi, and Young (2002)). Shu, King, and Fleck (1999) and Tsepoura, Papargyri-Beskou, and Polyzos (2002) were the first to use the finite element method (FEM) and the boundary element method (BEM), respectively, for solving elastostatic prob-

lems in the framework of the gradient elasticity theories of Mindlin. Since then many papers dealing with numerical solutions of gradient elastic problems have appeared in the literature. Here one can mention the FEM formulations of Amanatidou and Aravas (2002), Amanatidou, Giannakopoulos, and Aravas (2005), Engel, Garikipati, Hughes, Larson, Mazzei, and Taylor (2002), Tenek and Aifantis (2002), Peerlings and Fleck (2004), Soh and Wanji (2004), Imatani, Hataday, and Maugin (2005), Askes and Gutierrez (2006), Dessouky, Masad, Zbib, and Little (2003), Dessouky, Masad, Little, and Zbib (2006), Akarapu and Zbib (2006), Wei (2006) and Markolefas, Tsouvalas, and Tsamasphyros (2007), the BEM formulations of Tsepoura and Polyzos (2003), Polyzos, Tsepoura, Tsinopoulos, and Beskos (2003), Tsepoura, Tsinopoulos, Polyzos, and Beskos (2003), Polyzos, Tsepoura, and Beskos (2005) and Polyzos (2005) and the meshless local Petrov-Galerkin formulation of Tang, Shen, and Atluri (2003). In the aforementioned works, only those of Amanatidou and Aravas (2002), Imatani, Hataday, and Maugin (2005), Wei (2006) and Akarapu and Zbib (2006) are referred to the solution of gradient elastic fracture mechanics problems. More precisely, Amanatidou and Aravas (2002) proposing a two dimensional mixed FEM formulation for Mindlin's Form-I, II and III theory, solve the mode-III crack problem providing results for the antiplane stress and displacement fields around the tip of the crack. Although their findings are in agreement with the theoretical ones of Georgiadis (2003), there are no results dealing with the mode-III SIF or correlating the SIF with the constants associated with the considered gradient elastic model. Imatani, Hataday, and Maugin (2005) utilize a mixed Form-I FEM formulation for the solution of a plane mode-I crack problem providing results dealing with the variation of the energy release rate with respect to the length of the crack and only for specific values of the gradient elastic constants of the Form-I Mindlin's theory. Finally, Wei (2006) and Akarapu and Zbib (2006) using a mixed FEM formulation for the simplified Form-II and Fleck and Hutchinson (1997) gradient elastic theories, respectively, they calculate stresses and displacements near the tip of mode-I, II, III cracks without giving any information about the SIF and its dependence on the considered gradient elastic constants. Very recently, Karlis, Tsinopoulos, Polyzos, and Beskos (2007) developed a numerical methodology, which combines the BEM proposed by Polyzos, Tsepoura, Tsinopoulos, and Beskos (2003) and Tsepoura, Tsinopoulos, Polyzos, and Beskos (2003) with special crack tip boundary elements for the numerical determination of the SIF in mode-I and mixed mode-(I & II) fracture mechanics plane gradient elastic problems. Adopting the idea of variable-order singularity boundary elements around the tip of the crack for the evaluation of the corresponding SIF (Lim, Lee, Tay, and Zhou (2002)), a new special variable-order singularity discontinuous element was proposed for the treatment of singular fields around the tip of the crack. The SIFs determination was accomplished by a displacement type of formulation in connection with the multiregion approach. As it is mentioned in the review papers of Beskos (1997), Aliabadi (1997) and Dominguez and Ariza (2003), the displacement based BEM has the disadvantage of subregioning but is associated with lower order singularity kernels than either the traction or the dual BEM. On the other hand, it is well known that the BEM, as it is applied to linear elastic fracture mechanics, possesses some distinct advantages over the FEM as the dimensionality reduction of the problem, no requirements for remeshing and the higher level of accuracy achieved. These advantages are more pronounced in gradient elastic problems as the BEM does not have any continuity problem like the FEM, which, in order to deal with $C^{(1)}$ continuity problems, develops $C^{(0)}$ continuity mixed elements with a large number of degrees of freedom.

The goal of the present work is twofold: first to provide some new results dealing with two-dimensional (2D) mode-I gradient elastic cracks and second to extend the work of Karlis, Tsinopoulos, Polyzos, and Beskos (2007) to solve three dimensional mode-I gradient elastic fracture mechanics problems. The paper is organized as follows: the simplified Form-II gradient elastic

theory and how it is obtained from the most general Mindlin's Form-II theory is presented in the next section. The two-dimensional (2D) special variable order singularity discontinuous element and its extension to three dimensions are illustrated in section 3. The 2D and three-dimensional (3D) BEM employed for the needs of the present paper as well as the solution procedure for the computation of SIFs are reported in section 4. Finally, results concerning 2D and 3D mode-I crack problems are presented and discussed in sections 5 and 6.

2 Simplified Form II Gradient Elastic Theory: Theoretical Background

Mindlin in the Form-II version of his gradient elastic theory (Mindlin (1964)) considered that the potential energy density $\hat{W}$ is a quadratic form of the strains and the gradient of strains, i.e.

$$\hat{W} = \frac{1}{2}\lambda\varepsilon_{ii}\varepsilon_{jj} + \mu\varepsilon_{ij}\varepsilon_{ij} + \hat{\alpha}_1\hat{\kappa}_{iik}\hat{\kappa}_{kjj} + \hat{\alpha}_2\hat{\kappa}_{ijj}\hat{\kappa}_{ikk} + \hat{\alpha}_3\hat{\kappa}_{iik}\hat{\kappa}_{jjk} + \hat{\alpha}_4\hat{\kappa}_{ijk}\hat{\kappa}_{ijk} + \hat{\alpha}_5\hat{\kappa}_{ijk}\hat{\kappa}_{kji} \tag{1}$$

where $\varepsilon_{ij} = (\partial_i u_j + \partial_j u_i)/2$, $\hat{\kappa}_{ijk} = \partial_i\varepsilon_{jk} = (\partial_i\partial_j u_k + \partial_i\partial_k u_j)/2 = \hat{\kappa}_{ikj}$ and λ, μ, $\hat{\alpha}_1 \div \hat{\alpha}_5$ material constants. It should be noticed, however, that the constants λ, μ are not the same with the corresponding Lamè ones of the classical elasticity. Strains ε_{ij} and gradients of strains $\hat{\kappa}_{ijk}$ are dual in energy with the Cauchy and double stresses, respectively, defined as

$$\hat{\tau}_{ij} = \frac{\partial\hat{W}}{\partial e_{ij}} = \hat{\tau}_{ji} \tag{2}$$

$$\hat{\mu}_{ijk} = \frac{\partial\hat{W}}{\partial\hat{\kappa}_{ijk}} = \hat{\mu}_{ikj} \tag{3}$$

which implies that

$$\hat{\tau}_{pq} = 2\mu e_{pq} + \lambda e_{ii}\delta_{pq} \tag{4}$$

and

$$\hat{\mu}_{pqr} = \frac{1}{2}\hat{a}_1\left[\hat{k}_{rii}d_{pq} + 2\hat{k}_{iip}d_{qr} + \hat{k}_{qii}d_{rp}\right] + 2\hat{a}_2\hat{k}_{pii}d_{qr} + \hat{a}_3(\hat{k}_{iir}d_{pq} + \hat{k}_{iiq}d_{pr}) + 2\hat{a}_4\hat{k}_{pqr} + \hat{a}_5\left(\hat{k}_{rpq} + \hat{k}_{qrp}\right) \tag{5}$$

or in dyadic form

$$\hat{\tau} = \mu(\nabla\mathbf{u} + \mathbf{u}\nabla) + \lambda(\nabla\cdot\mathbf{u})\mathbf{I} \tag{6}$$

$$\begin{aligned}\hat{\mu} = {} & \frac{1}{2}\hat{\alpha}_1[\nabla^2\mathbf{u}\otimes\mathbf{I} + \mathbf{I}\otimes\nabla\nabla\cdot\mathbf{u} \\ & + \nabla\nabla\cdot\mathbf{u}\otimes\mathbf{I} + (\nabla\nabla\cdot\mathbf{u}\otimes\mathbf{I})^{213}] \\ & + 2\hat{\alpha}_2\nabla\nabla\cdot\mathbf{u}\otimes\mathbf{I} \\ & + \frac{1}{2}\hat{\alpha}_3[\mathbf{I}\otimes\nabla^2\mathbf{u} + \mathbf{I}\otimes\nabla\nabla\cdot\mathbf{u} \\ & + \left(\nabla^2\mathbf{u}\otimes\mathbf{I}\right)^{213} + (\nabla\nabla\cdot\mathbf{u}\otimes\mathbf{I})^{213}] \\ & + \hat{\alpha}_4(\nabla\nabla\mathbf{u} + \nabla\mathbf{u}\nabla) \\ & + \frac{1}{2}\hat{\alpha}_5(2\mathbf{u}\nabla\nabla + \nabla\nabla\mathbf{u} + \nabla\mathbf{u}\nabla)\end{aligned} \tag{7}$$

with $\otimes$ denoting dyadic product of two vectors, $\mathbf{I}$ being the second order unit tensor and $(\mathbf{a}\otimes\mathbf{b}\otimes\mathbf{c})^{213} = \mathbf{b}\otimes\mathbf{a}\otimes\mathbf{c}$

The first subscript of the double stress tensor μ_{ikj} indicates the normal vector on the surface on which the double stresses act, while the other two have the same significance as the corresponding ones of the classical stress tensor τ_{ij}. As it is explained by Georgiadis (2003), double stresses are nonvanishing stresses produced by internal self-equilibrating forces. A practical example of double forces is presented in the recent work of Vardoulakis and Giannakopoulos (2006).

Ignoring body forces, considering smooth boundaries and taking the variation of (1), one obtains from the resulting variational statement the equilibrium equation

$$\partial_j\sigma_{jk} = \partial_j(\hat{\tau}_{jk} - \partial_i\hat{\mu}_{ijk}) = 0 \tag{8}$$

accompanied by the boundary conditions

$$u_k = \overline{u} \text{ and/or } \hat{P}_k = \overline{p} \tag{9}$$

$$n_l\partial_l u_k = \overline{q} \text{ and/or } \hat{R}_k = \overline{R} \tag{10}$$

where $\sigma_{jk}, \hat{\tau}_{jk}, -\partial_i\hat{\mu}_{ijk}$ represent the symmetric total, Cauchy and relative stress tensors, respectively, $\overline{u}, \overline{p}, \overline{q}, \overline{R}$ are prescribed vectors, n_k is the unit vector normal to the boundary and $\hat{P}_k, \hat{R}_k$ are the traction and double traction vectors, respectively, having the form

$$\hat{P}_k = n_j\hat{\tau}_{jk} - n_i n_j D\hat{\mu}_{ijk} - (n_j D_i + n_i D_j)\hat{\mu}_{ijk} + (n_i n_j D_l n_l - D_j n_i)\hat{\mu}_{ijk} \tag{11}$$

$$\hat{R}_k = n_i n_j\hat{\mu}_{ijk} \tag{12}$$

or in dyadic form

$$\begin{aligned}\hat{\mathbf{P}} &= \hat{\mathbf{n}}\cdot\hat{\tau} - (\hat{\mathbf{n}}\otimes\hat{\mathbf{n}}) : \partial_n\hat{\mu} - \hat{\mathbf{n}}\cdot(\nabla_S\cdot\hat{\mu}) \\ &\quad - \hat{\mathbf{n}}\cdot(\nabla_S\cdot\hat{\mu}^{213}) + (\nabla_S\cdot\hat{\mathbf{n}})(\hat{\mathbf{n}}\otimes\hat{\mathbf{n}}) : \hat{\mu} \\ &\quad - (\nabla_S\hat{\mathbf{n}}) : \hat{\mu} \end{aligned} \tag{13}$$

$$\hat{\mathbf{R}} = \hat{\mathbf{n}}\cdot\hat{\mu}\cdot\hat{\mathbf{n}} \equiv (\hat{\mathbf{n}}\otimes\hat{\mathbf{n}}) : \hat{\mu} \tag{14}$$

where $D_i = \partial_i - n_i n_k \partial_k$, $D = n_l\partial_l$ and $\nabla_s = (\mathbf{I} - \hat{\mathbf{n}}\otimes\hat{\mathbf{n}})\cdot\nabla$. Inserting (4) and (5) into (8) one obtains the equilibrium equation of a Form-II gradient elastic material written in terms of displacements as

$$\begin{aligned}&(\lambda+2\mu)(1-\hat{l}_1^2\nabla^2)\nabla\nabla\cdot\mathbf{u} \\ &-\mu(1-\hat{l}_2^2\nabla^2)\nabla\times\nabla\times\mathbf{u} = \mathbf{0}\end{aligned} \tag{15}$$

where

$$\begin{aligned}\hat{l}_1^2 &= 2\left(\hat{\alpha}_1+\hat{\alpha}_2+\hat{\alpha}_3+\hat{\alpha}_4+\hat{\alpha}_5\right)/\left(\lambda+2\mu\right) \\ \hat{l}_2^2 &= \left(\hat{\alpha}_3+\hat{\alpha}_4+\hat{\alpha}_5\right)/2\mu\end{aligned} \tag{16}$$

Rearranging (15) and considering that λ, μ represent the Lamè constants, it is easy to see that

$$\begin{aligned}&(\lambda+2\mu)\nabla\nabla\cdot\mathbf{u} - \mu\nabla\times\nabla\times\mathbf{u} \\ &-\hat{l}_1^2\nabla^2\left[(\lambda+2\mu)\nabla\nabla\cdot\mathbf{u} - \mu\nabla\times\nabla\times\mathbf{u}\right] \\ &+\mu(\hat{l}_2^2-\hat{l}_1^2)\nabla^2(\nabla\times\nabla\times\mathbf{u}) = \mathbf{0}\end{aligned} \tag{17}$$

or in terms of classical elasticity

$$\begin{aligned}&[\text{Classical Elastic Equilibrium Eq.}] \\ &-\hat{l}_1^2\nabla^2\,[\text{Classical Elasticity Equilibrium Eq.}] \\ &+\tilde{\mu}\left(\hat{l}_2^2-\hat{l}_1^2\right)\nabla^2\left(\nabla\times\nabla\times\mathbf{u}\right) = \mathbf{0}\end{aligned} \tag{18}$$

Although very elegant, the use of the Form II gradient elastic theory for the solution of real problems is discouraging since seven new material constants, i.e. λ, μ, $\hat{\alpha}_1 \div \hat{\alpha}_5$ have to be determined. If the constants $\hat{\alpha}_1 \div \hat{\alpha}_5$ take the values

$$\begin{aligned}\hat{\alpha}_1 &= \hat{\alpha}_3 = \hat{\alpha}_5 = 0 \\ \hat{\alpha}_2 &= (\lambda/2)\,g^2 \\ \hat{\alpha}_4 &= \mu g^2\end{aligned} \tag{19}$$

then the constitutive equations (6), (7) as well as the equilibrium equation (17) can be written as

$$\hat{\tau} = \mu(\nabla\mathbf{u}+\mathbf{u}\nabla) + \lambda(\nabla\cdot\mathbf{u})\mathbf{I} \tag{20}$$

$$\hat{\mu} = g^2\nabla\hat{\tau} \tag{21}$$

$$\begin{aligned}&(\lambda+2\mu)\nabla\nabla\cdot\mathbf{u} - \mu\nabla\times\nabla\times\mathbf{u} \\ &-g^2\nabla^2\left[(\lambda+2\mu)\nabla\nabla\cdot\mathbf{u} - \mu\nabla\times\nabla\times\mathbf{u}\right] = \mathbf{0}\end{aligned} \tag{22}$$

where λ, μ are the classical Lamè constants and g^2 is the volumetric strain gradient energy coefficient or simply the gradient coefficient, which is introduced to balance the dimensions of strains and strain gradients and moreover to relate the microstructure with the macrostructure representing a characteristic length of the material. Thus, as it is stated in Vardoulakis, Exadaktylos, and Aifantis (1996), the gradient elastic theory described by Eqs (20-22) is the simplest possible special case of Mindlin's theory. As it has already been mentioned, the present work exploits this simple enhanced elastic theory, which from now will be reffered to as Mindlin's simplified Form-II gradient elastic theory.

3 Unified 2D and 3D discontinuous elements of variable-order singularity

Karlis, Tsinopoulos, Polyzos, and Beskos (2007) proposed a new variable singularity element suitable for representing fields developed near the crack tip of a 2D gradient elastic solid. In the present section a new 3D variable singularity element is proposed and both 2D and 3D special elements are presented in a unified way. According to Vardoulakis, Exadaktylos, and Aifantis (1996), Exadaktylos, Vardoulakis, and Aifantis (1996), Vardoulakis and Exadaktylos (1997), Exadaktylos (1998), Zhang, Huang, Chen, and Hwang (1998), Shi, Huang, and Hwang (2000), Fannjiang, Chan, and Paulino (2002), Georgiadis (2003) and Radi (2008), the fields **u**, **q**, **R** and **P** near the crack tip vary as $r^{3/2}$, $r^{1/2}$, $r^{-1/2}$ and $r^{-3/2}$ respectively, with r being the distance from the tip. As it is well known, the elements used in a classical BEM formulation interpolate the unknown fields either linearly or quadratically and therefore the behavior of the fields around the crack tip can never be

represented correctly. In the present work, adopting the idea of using variable-order singularity continuous boundary elements around the tip or the front of the crack for the description of the near tip behavior and the evaluation of the corresponding SIFs as described in Lim, Lee, Tay, and Zhou (2002) and Zhou, Lim, Lee, and Tay (2005), special variable-order of singularity discontinuous line and quadrilateral boundary elements for 2D and 3D analyses, respectively, are proposed.

Thus, e.g., for the special elements of the 3d cases the crack side is always discontinuous, while discontinuity on the other sides is optional. The main advantage of using discontinuity at the crack side is that no functional nodes are located at the crack front and thus, despite the singularity of **R** and **P** there, the field nodal values are finite and can be computed.

3.1 2D discontinuous elements of variable-order singularity

The local coordinates of the functional nodes of the special element are identical to those of a classical, partially or fully discontinuous, 3-noded, quadratic line element. As shown in Fig. 1, the tip of the crack can be located either at $\xi = -1$ or at $\xi = 1$ for the special element being to the left or right of the tip. In order to unify these two possible cases a new variable p is introduced via the linear transformation

$$p = (1 + c\xi)/2 \tag{23}$$

with $c = \pm 1$ for the tip located at $\xi = \mp 1$, respectively. Thus, the tip of the crack is always located at $p = 0$ and the interval $\xi \in [-1, 1]$ is transformed into the interval $p \in [0, 1]$. After the transformation, the tip of the crack is located at $p = 0$ (Fig. 2). Consider a point $\mathbf{x}(p)$ on the element and a point $\mathbf{y}(0)$ located at the crack tip. The fields of interest **F** at the point **x**, can be expressed in terms of the asymptotic solutions as

$$\mathbf{F} = \mathbf{K}r^{\lambda_1} + \mathbf{L}r^{\lambda_2} + \mathbf{C} \tag{24}$$

where **K**, **L** and **C** are constant vectors to be determined. Vector **F** could represent **u**, **q**, **R** or **P** and

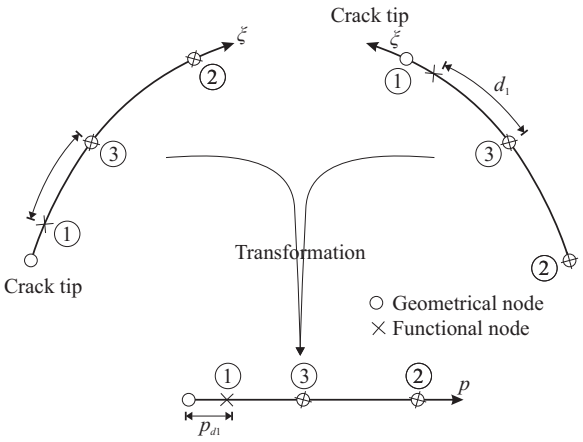

Figure 1: Variable order of singularity discontinuous boundary element and its transformation.

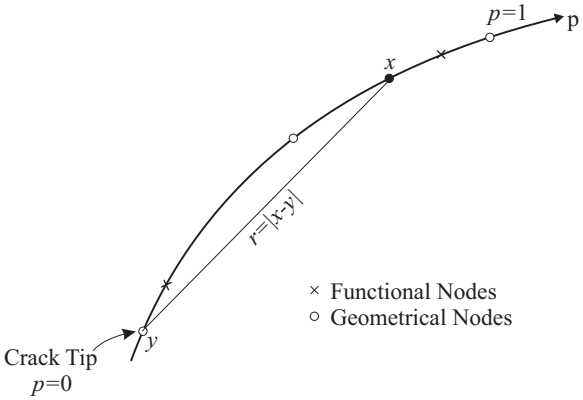

Figure 2: A 2D, discontinuous, variable order of singularity element.

thus λ_1 and λ_2 take the values displayed in Tab. 1. Considering that suitable interpolation functions N^i exist, fields **F** can be approximated as

$$\mathbf{F} = N^i \mathbf{F}^i \quad i=1,2,3 \tag{25}$$

with $\mathbf{F}^i$ being the three nodal values of **F**. In view of Eq. (24) N^i should have the form

$$N^i(r; p, \lambda_1, \lambda_2) = a^i r^{\lambda_1} + b^i r^{\lambda_2} + z^i \tag{26}$$

where $r = \left| x^j(p) - y(0) \right|$ is the distance of the functional node j from the crack tip, as illustrated in Fig. 2, while the vectors **K**, **L**, **C** of Eq. (24)

are given by

$$\begin{aligned}\mathbf{K} &= a^i\mathbf{F}^i\\ \mathbf{L} &= b^i\mathbf{F}^i\\ \mathbf{C} &= z^i\mathbf{F}^i\end{aligned} \tag{27}$$

The constants a^i, b^i, z^i can be easily obtained by solving a set of three linear systems, consisting of three equations each, which arise from the requirement that each interpolation function must satisfy the relations

$$N^i\,(p \text{ corresponding to node } j) = \delta_{ij} \quad i,j=1,2,3 \tag{28}$$

where δ_{ij} is the Kronecker delta. It can be verified that $\sum N^i = 1$ for all the combinations of λ_1, λ_2 provided in Tab. 1. Finally it should be mentioned that the present 2D element formulation is more accurate than the one reported in Karlis, Tsinopoulos, Polyzos, and Beskos (2007) since the distance r between points **x** and **y** (Fig. 2) is taken here as a straight line between these points as it should be and not as a curved one along the coordinate p, as it was the case in Karlis, Tsinopoulos, Polyzos, and Beskos (2007).

Table 1: Orders of magnitude of the asymptotic fields.

F	λ_1	λ_2
u	$3/2$	1
q	$1/2$	1
R	$-1/2$	1
P	$-3/2$	$-1/2$

3.2 3D discontinuous elements of variable-order singularity

As in the 2D case, near the crack front, the fields **u**, **q**, **R** and **P** vary as $r^{3/2}$, $r^{1/2}$, $r^{-1/2}$ and $r^{-3/2}$ respectively, with r being the distance from the crack front. Once more, adopting the idea of using variable-order continuous elements (Lim, Lee, Tay, and Zhou (2002) and Zhou, Lim, Lee, and Tay (2005)), a new discontinuous, quadrilateral, eight-nodded element with variable-order singularity is proposed for the treatment of the fields around the crack front. In this special element, the crack side is always discontinuous, while discontinuity on the other sides is optional. The main advantage of using discontinuity on the crack side is that no functional nodes are located on the crack front and thus, despite the singularity of **R** and **P** there, the field nodal values are finite and can be computed. The local coordinates of the functional nodes are identical to those of a classical, partially or fully discontinuous, eight-nodded, quadratic, quadrilateral element. Practically, the crack front can be located at any of the element's sides. In order to be able to deal with all the possible cases of the crack front location, the local numbering of the element nodes is changed, so that the crack front always resides on the first side of the element. The result of the local renumbering is described in Tab. 2 for all the possible cases.

Table 2: The renumbering of the element nodes, so that the crack front always resides on the first side.

Nodes	Crack on:			
	Side 1	Side 2	Side 3	Side 4
Node $1'$	1	2	3	4
Node $2'$	2	3	4	1
Node $3'$	3	4	1	2
Node $4'$	4	1	2	3
Node $5'$	5	6	7	8
Node $6'$	6	7	8	5
Node $7'$	7	8	5	6
Node $8'$	8	5	6	7
Local coord. ξ_1'	ξ_1	ξ_2	$-\xi_1$	$-\xi_2$
Local coord. ξ_2'	ξ_2	$-\xi_1$	$-\xi_2$	ξ_1

An example of an element having the crack front located at its third side is illustrated in Fig. 3. Consider a point $\mathbf{x}(\xi_1',\xi_2')$ on the element and a point $\mathbf{y}(\xi_1',-1)$ located at the crack front having the same ξ_1-coordinate as x, as shown in Fig. 4. The field of interest **F** at the point **x**, can be ex-

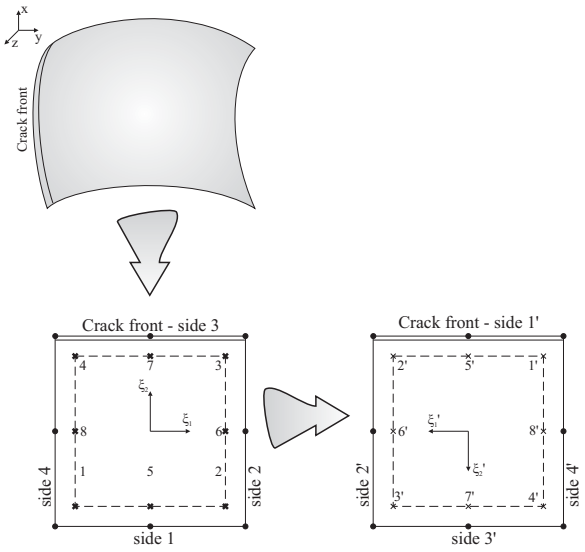

Figure 3: Transition from the real 3D space to the parametric representation of the element and nodal renumbering, for the case of a fully discontinuous element.

pressed in terms of the asymptotic solutions as

$$\mathbf{F}\left(\xi_1', r\right) = \mathbf{K}\left(\xi_1'\right) r^{\lambda_1} + \mathbf{L}\left(\xi_1'\right) r^{\lambda_2} + \mathbf{C}\left(\xi_1'\right) \quad (29)$$

where r is the distance $r = |\mathbf{x} - \mathbf{y}|$, the symbol $\mathbf{F}$ represents $\mathbf{u}$, $\mathbf{q}$, $\mathbf{R}$ and $\mathbf{P}$ and λ_1, λ_2 take the values of Tab. 1. In addition, the fields $\mathbf{F}$ can be approximated using the interpolation functions N^i and their corresponding nodal values $\mathbf{F}^i$ as follows:

$$\mathbf{F}\left(\xi_1', r\right) = N^i\left(\xi_1', r\right)\mathbf{F}^i, i = 1,...,8 \quad (30)$$

Combining Eqs (29) and (30) and assuming a quadratic behaviour for the functions $\mathbf{K}(\xi_1')$, $\mathbf{L}(\xi_1')$ and $\mathbf{C}(\xi_1')$, the interpolation functions N^i should be of the form

$$\begin{aligned} N^i\left(\xi_1', r\right) = &\left(e_1^i + e_2^i \xi_1' + e_3^i \xi_1'^2\right) r^{\lambda_1} \\ &+ \left(e_4^i + e_5^i \xi_1 + e_6^i \xi_1'^2\right) r^{\lambda_2} \\ &+ e_7^i + e_8^i \xi_1' + e_9^i \xi_1'^2 \end{aligned} \quad (31)$$

where e_j^i, $(j = 1,...,9)$ are constants to be determined. Due to the use of eight-noded elements, one of the nine terms of the above expression must be omitted. In the present work, having in mind that the coefficients of r^{λ_1} and r^{λ_2} will be used

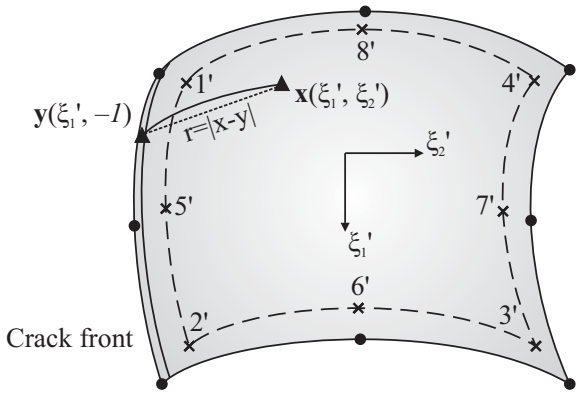

Figure 4: Projection of point x to the crack front.

for the SIF calculation, this term is taken to be e_9^i . The remaining eight constants e_j^i can be easily obtained by solving a set of eight linear systems, consisting of eight equations each, which arise from the requirement that each interpolation function N^i must satisfy the relations

$$N^i\left(\xi_1'^j, r^j\right) = \delta_{ij}, \mathrm{i}, j = 1,...,8 \quad (32)$$

where δ_{ij} is the Kronecker delta, $r^j = |\mathbf{x}\left(\xi_1'^j, \xi_2'^j\right) - \mathbf{y}\left(\xi_1'^j, -1\right)|$ and $\left(\xi_1'^j, \xi_1'^j\right)$ are the local coordinates of the j functional node. It can be verified that $\sum N^i = 1$ for all the combinations of λ_1, λ_2 provided in Tab. 2.

4 BEM Procedure and SIF Determination

In this section the 2D and 3D BEM procedure is presented in brief and the evaluation of the corresponding SIFs via the nodal values of the special elements is explained. Adopting the simplified Mindlin's Form-II gradient elastic theory and utilizing the well known identity $\nabla^2 = \nabla\nabla\cdot - \nabla\times\nabla\times$ the equilibrium equation (22) obtains the more familiar form

$$\begin{aligned} &\mu\nabla^2\mathbf{u} + (\lambda+\mu)\nabla\nabla\cdot\mathbf{u} \\ &\quad - g^2\nabla^2\left(\mu\nabla^2\mathbf{u} + (\lambda+\mu)\nabla\nabla\cdot\mathbf{u}\right) = \mathbf{0} \end{aligned} \quad (33)$$

As it is proved in Polyzos, Tsepoura, Tsinopoulos, and Beskos (2003), the fundamental solution of

(33) has the form

$$\tilde{\mathbf{u}}^*(r;\mu,\nu,g) = \frac{1}{16\pi\mu(1-\nu)}\left[\Psi(r;\nu,g)\tilde{\mathbf{I}} - \mathrm{X}(r;g)\,\hat{\mathbf{r}}\otimes\hat{\mathbf{r}}\right] \quad (34)$$

where ν is the Poisson ratio, $\hat{r}$ the unit vector in the direction $\mathbf{r}=\mathbf{y}-\mathbf{x}$, $r=|y-x|$ and X, Ψ scalar functions given for the 2D and 3D cases, respectively by the relations

$$\mathrm{X} = -2+\frac{8g^2}{r^2}-4\mathrm{K}_2(r/g) \quad (35)$$

$$\Psi = -2(3-4\nu)\ln r+\frac{4g^2}{r^2} -2(3-4\nu)\mathrm{K}_0(r/g)-2\mathrm{K}_2(r/g) \quad (36)$$

and

$$X(r,g) = -\frac{1}{r}+\frac{6g^2}{r^3}-\left(\frac{6g^2}{r^3}+\frac{6g}{r^2}+\frac{2}{r}\right)e^{-r/g} \quad (37)$$

$$\Psi(r,\nu,g) = (3-4\nu)\frac{1}{r} +2(1-2\nu)\left[-\frac{g^2}{r^3}+\left(\frac{g^2}{r^3}+\frac{g}{r^2}\right)e^{-r/g}\right] +4(1-\nu)\left[\frac{g^2}{r^3}+\left(\frac{g^2}{r^3}+\frac{g}{r^2}+\frac{1}{r}\right)e^{-r/g}\right] \quad (38)$$

with $K_0(.)$ and $K_2(.)$ being the modified Bessel functions of the second kind and zero and second order, respectively. Considering a gradient elastic material of volume V surrounded by a smooth boundary S and characterized by two Lamè constants λ,μ and a gradient coefficient g^2, Polyzos, Tsepoura, Tsinopoulos, and Beskos (2003) showed that for any static gradient elastic boundary value problem its integral representation reads

$$\tilde{\mathbf{c}}(\mathbf{x})\cdot\mathbf{u}(\mathbf{x}) + \int_S \left\{\tilde{\mathbf{P}}^*(\mathbf{x},\mathbf{y})\cdot\mathbf{u}(\mathbf{y})-\tilde{\mathbf{u}}^*(\mathbf{x},\mathbf{y})\cdot\mathbf{P}(\mathbf{y})\right\}dS_{\mathbf{y}} = \int_S \left\{\frac{\partial\tilde{\mathbf{u}}^*(\mathbf{x},\mathbf{y})}{\partial n_{\mathbf{y}}}\cdot\mathbf{R}(\mathbf{y})-\tilde{\mathbf{R}}^*(\mathbf{x},\mathbf{y})\cdot\mathbf{q}(\mathbf{y})\right\}dS_{\mathbf{y}} \quad (39)$$

where $\tilde{\mathbf{u}}^*(\mathbf{x},\mathbf{x})$ is the fundamental solution given by Eq. (34), $\tilde{\mathbf{P}}^*(\mathbf{x},\mathbf{x})$ and $\tilde{\mathbf{R}}^*(\mathbf{x},\mathbf{x})$ are the fundamental traction and double stress traction tensors, respectively and $\tilde{\mathbf{c}}(\mathbf{x})$ is the well-known jump tensor being equal to $(1/2)\tilde{\mathbf{I}}$ for $\mathbf{x}\in S$ and equal to $\tilde{\mathbf{I}}$ when $\mathbf{x}\in V\cap S$. Observing Eq. (39), one realizes that this equation contains four unknown vector fields, $\mathbf{u}(\mathbf{x})$, $\mathbf{P}(\mathbf{x})$, $\mathbf{R}(\mathbf{x})$ and $\mathbf{q}(\mathbf{x})=\partial\mathbf{u}/\partial n$. Thus, the evaluation of the unknown fields requires the existence of one more integral equation. This integral equation is obtained by applying the operator $\partial/\partial n_x$ on Eq. (39) and has the form

$$\tilde{\mathbf{c}}(\mathbf{x})\cdot\frac{\partial\mathbf{u}(\mathbf{x})}{\partial n_{\mathbf{x}}}+ \int_S\left\{\frac{\partial\tilde{\mathbf{P}}^*(\mathbf{x},\mathbf{y})}{\partial n_{\mathbf{x}}}\cdot\mathbf{u}(\mathbf{y})-\frac{\partial\tilde{\mathbf{u}}^*(\mathbf{x},\mathbf{y})}{\partial n_{\mathbf{x}}}\cdot\mathbf{P}(\mathbf{y})\right\}\cdot dS_{\mathbf{y}} = \int_S\left\{\frac{\partial^2\tilde{\mathbf{u}}^*(\mathbf{x},\mathbf{y})}{\partial n_{\mathbf{x}}\partial n_{\mathbf{y}}}\cdot\mathbf{R}(\mathbf{y})-\frac{\partial\tilde{\overline{\mathbf{R}}}^*(\mathbf{x},\mathbf{y})}{\partial n_{\mathbf{x}}}\cdot\mathbf{q}(\mathbf{y})\right\}\cdot dS_{\mathbf{y}} \quad (40)$$

All the kernels appearing in the integral equations (39) and (40) are given explicitly in Polyzos, Tsepoura, Tsinopoulos, and Beskos (2003). Integral equations (39) and (40) accompanied by the classical and non-classical boundary conditions (9) and (10) form the integral representation of the general gradient elastic boundary value problem. The goal of the BEM is to solve numerically the just described well-posed boundary value problem. To this end the global boundary S is discretized into quadratic, continuous and discontinuous isoparametric boundary elements, while special variable-order singularity, discontinuous elements are placed on both sides of the crack tip or crack front as it is illustrated in Fig. 5. Then, for a node k the integral Eqs (39) and (40) are written as

$$\frac{1}{2}\mathbf{u}^k+\sum_{\beta=1}^{M}\tilde{\mathbf{H}}_\beta^k\cdot\mathbf{u}^\beta+\sum_{\beta=1}^{M}\tilde{\mathbf{K}}_\beta^k\cdot\mathbf{q}^\beta = \sum_{\beta=1}^{M}\tilde{\mathbf{G}}_\beta^k\cdot\mathbf{P}^\beta+\sum_{\beta=1}^{M}\tilde{\mathbf{L}}_\beta^k\cdot\mathbf{R}^\beta$$

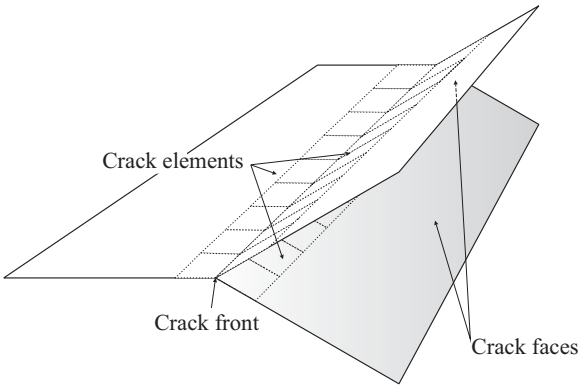

Figure 5: Position of the variable order of singularity elements.

$$\frac{1}{2}\mathbf{q}^k + \sum_{\beta=1}^{M} \tilde{\mathbf{S}}_\beta^k \cdot \mathbf{u}^\beta + \sum_{\beta=1}^{M} \tilde{\mathbf{T}}_\beta^k \cdot \mathbf{q}^\beta = \sum_{\beta=1}^{M} \tilde{\mathbf{V}}_\beta^k \cdot \mathbf{P}^\beta + \sum_{\beta=1}^{M} \tilde{\mathbf{W}}_\beta^k \cdot \mathbf{R}^\beta \quad (41)$$

where M is the total number of nodes. Explicit expressions for $\tilde{\mathbf{H}}_\beta^k, \tilde{\mathbf{K}}_\beta^k, \tilde{\mathbf{G}}_\beta^k, \tilde{\mathbf{L}}_\beta^k, \tilde{\mathbf{S}}_\beta^k, \tilde{\mathbf{T}}_\beta^k, \tilde{\mathbf{V}}_\beta^k$ and $\tilde{\mathbf{W}}_\beta^k$ are given in Tsepoura, Tsinopoulos, Polyzos, and Beskos (2003).

Collocating Eqs (41) at all nodal points M and applying the boundary conditions (Eqs (9) and (10)) one produces the final linear system of algebraic equations of the form $\tilde{\mathbf{A}} \cdot \mathbf{X} = \mathbf{B}$, where the vectors $\mathbf{X}$ and $\mathbf{B}$ contain all the unknown and known nodal components of the boundary fields, respectively. The singular and hypersingular integrals involved, are evaluated with high accuracy by applying a methodology for direct treatment of CPV and hypersingular integrals explained in Tsepoura, Tsinopoulos, Polyzos, and Beskos (2003). Near to the crack front, an extra singularity due to the singular behaviour of the interpolation functions (26) and (31) should be taken into account. The numerical treatment of all possible singular integrals defined on the considered special elements is presented for 2D and 3D in Karlis, Tsinopoulos, Polyzos, and Beskos (2007) and the appendix of the present paper, respectively. Finally, the linear system is solved via a typical LU-decomposition algorithm and the vector $\mathbf{X}$ comprising all the unknown nodal values of $\mathbf{u}$, $\mathbf{P}$, $\mathbf{R}$, $\mathbf{q}$ is evaluated. Once the boundary value problem has been solved, the calculation of SIFs is done via the nodal traction values of the special elements. Approaching the crack tip or front ($r \to 0$), the traction $\mathbf{P}$, according to Eq. (24) for the 2D case and Eq. (29) for the 3D case, admits a representation of the form

$$\mathbf{P} = \frac{\mathbf{K_1}(\mathbf{P_1}, ..., \mathbf{P}_N)}{\sqrt{2\pi}} \lim_{r\to 0} r^{-3/2} + \frac{\mathbf{K_2}(\mathbf{P_1}, ..., \mathbf{P}_N)}{\sqrt{2\pi}} \lim_{r\to 0} r^{-1/2} + \mathbf{C}(\mathbf{P_1}, ..., \mathbf{P}_N) \quad (42)$$

where $N = 3$ for 2D and $N = 8$ for 3D. Taking into account relation (27) and (31) the stress intensity factors corresponding to x, y and to x, y and z directions for 2D and 3D respectively, are obtained by

$$\mathbf{K}_1 = \sqrt{2\pi}\mathbf{K} = \sqrt{2\pi}\, a^j \mathbf{P}_j$$
$$\mathbf{K}_2 = \sqrt{2\pi}\mathbf{L} = \sqrt{2\pi}\, b^j \mathbf{P}_j \quad (43)$$

and

$$\mathbf{K}_1(\xi_1) = \sqrt{2\pi}\left(\mathbf{D}_1 + \xi_1 \mathbf{D}_2 + \xi_1^2 \mathbf{D}_3\right)$$
$$\mathbf{K}_2(\xi_1) = \sqrt{2\pi}\left(\mathbf{D}_4 + \xi_1 \mathbf{D}_5 + \xi_1^2 \mathbf{D}_6\right) \quad (44)$$

with $j = 1, 2, 3$ for two dimensions and $\mathbf{D}_i = e_i^j \mathbf{P}_j$, $i = 1, ..., 6$ and $j = 1, ..., 8$ for three dimensions and a^j, b^j, e_i^j calculated from solving the systems (28) and (32).

5 Numerical Results

Two mode-I fracture problems are studied in this section. The first deals with a 2D crack, while the second concerns a rectangular 3D crack both subjected to a tensile loading. The obtained crack profiles as well as the corresponding SIFs are presented and compared against those of classical elasticity.

5.1 2D Mode-I crack problem

Consider a square gradient elastic plate with rounded corners of very small radius of curvature (in order to have a smooth boundary) in a state of plane stress. The plate contains a central horizontal line crack and is subjected to a uniform tensile

traction $P_0 = 100$MPa applied normal to its top and bottom sides, as shown in Fig. 6. The crack length is chosen to be equal to $2a = 1$m and the side of the square plate is $L = 16a$. The Young modulus and the Poisson ratio of the gradient elastic plate are $E = 210$GPa and $\nu = 0.2$, respectively. Due to the double symmetry of the problem, only one quarter of the plate is discretized, with the following boundary conditions along the axes of symmetry: $\mathbf{P}(0,y) = \mathbf{0}$ and $\mathbf{R}(0,y) = \mathbf{0}$ for $0 \le y < a$, $u_y(0,y) = 0$ and $\mathbf{R}(0,y) = \mathbf{0}$ for $a \le y \le L/2$ and $u_x(x,0) = 0$ and $\mathbf{R}(x,0) = \mathbf{0}$ for $0 \le x \le L/2$. Fig. 7 displays the upper-right-

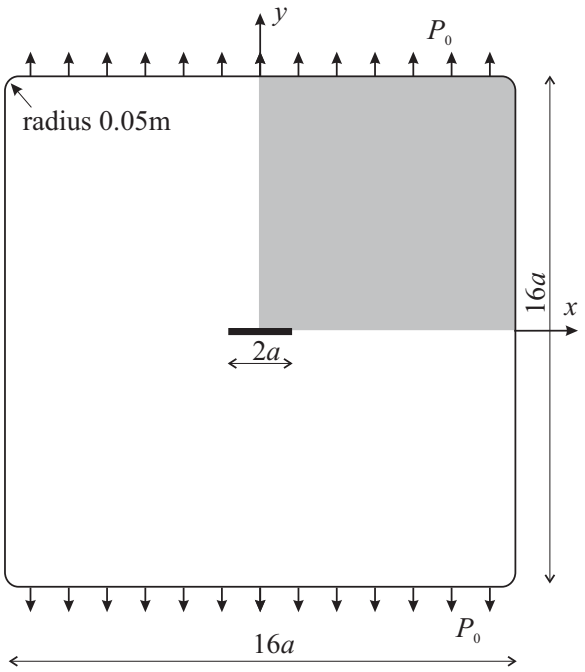

Figure 6: Gradient elastic plate with a horizontal line crack.

quarter of the crack opening displacement profile obtained by the present BEM for four different values of the gradient coefficient g (0.01, 0.1, 0.3, 0.5). In the same figure, the crack profile provided by the classical elasticity theory ($g = 0$) is also shown. As it is apparent, the crack profile in the gradient elastic case remains sharp at the crack tip and is not blunted as in the classical case. This cusp type of profile is identical to the one coming out of Barenblatt's (Barenblatt (1962)) cohesive zone theory. Barenblatt explains

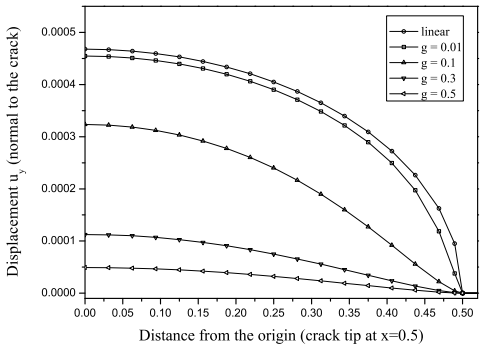

Figure 7: Upper right quarter of the COD profile.

that the two faces of the crack at the tip are subjected to very strong interatomic forces. Thus, considering these atomic attraction forces as compressive stresses larger than the tensile ones due to external loading, he obtained a cusp-like crack opening near the tip of the crack. The important conclusion here is that the results depicted in Fig. 7 are fully compatible with Barenblatt's findings without, however, to consider other forces than those implied by the Mindlin's simpilified Form-II gradient elastic theory. Also, it should be noticed that as the gradient coefficient g increases, the crack becomes stiffer. In Figs 8 and 9 the two

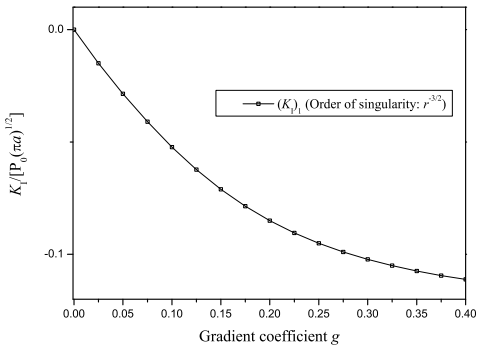

Figure 8: SIF $(K_I)_1$ as function of the gradient coefficient g.

mode-I SIFs for the gradient elastic case, $(K_I)_1$

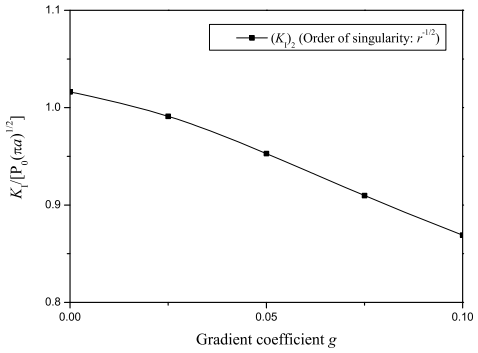

Figure 9: SIF $(K_I)_2$ as function of the gradient coefficient g.

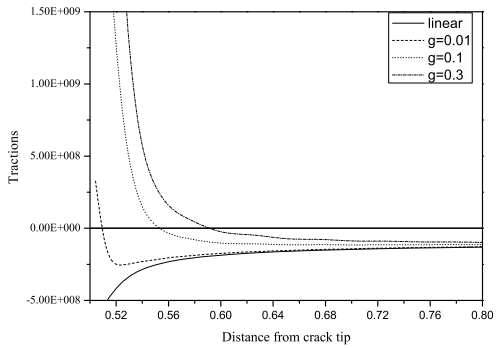

Figure 10: Traction values near the crack tip.

and $(K_I)_2$, are plotted versus the gradient coefficient g. The interesting remark here is that the SIF $(K_I)_1$ tends to zero as the gradient coefficient g tends to zero. As a result of that, Eq. (42) becomes $P_y = (K_I)_2 / \sqrt{2\pi} \lim_{r\to 0} r^{-1/2}$ with $(K_I)_2$ being the mode-I SIF as defined in classical elasticity theory. Moreover, Fig. 9 depicts the behavior of the SIF corresponding to $r^{-1/2}$ traction term as a function of the gradient elastic coefficient g. It should be noted that for g greater than 0.1 the contribution of this term is much smaller than that of the term corresponding to $r^{-3/2}$. For this reason the evaluation of the SIF $(K_I)_2$ for large g requires further investigation. However, for small g it is apparent from Fig. 9 that as g approaches zero $(K_I)_2$ becomes dominant and goes to the classical elastic case. However, the most important observation here is that the SIF $(K_I)_1$ takes only negative values. This means that in gradient elasticity the stresses near the crack tip not only go to infinity with a different order ($r^{-3/2}$) than those of classical elasticity ($r^{-1/2}$), but are also compressive and not tensile as in classical elasticity. This explains the different shapes of the crack profile in gradient and classical elasticity theories, as shown in Fig. 7. This behaviour becomes more pronounced in Fig. 10 where the traction field near to the crack tip, for various values of the gradient coefficient g is displayed.

5.2 3D Mode I Crack Problem

Consider a gradient elastic cube with rounded corners of very small radius of curvature (in order to have a smooth boundary). The cube contains a central horizontal rectangular crack and is subjected to a uniform tensile traction $P_0 = 100$MPa applied normal to its top and bottom sides. The side of the cube L is chosen to be equal to $16a = 8$ and the crack dimensions are $2a \times L$, as shown in Fig. 11. The Young modulus and the Poisson ratio of the gradient elastic plate are $E = 210$GPa and $\nu = 0.2$, respectively. Due to the octant symmetry of the problem, the analysis is performed by taking into acount two Cartesian symmetries with respect to the X-Z and Y-Z planes, while on the X-Y symmetry plane the following boundary conditions are considered: $\mathbf{P}(x,y,0) = \mathbf{0}$ and $\mathbf{R}(x,y,0) = \mathbf{0}$ for $0 \le x < a$ and $0 \le y < L/2$ and $u_z(x,y,0) = 0$ and $\mathbf{R}(x,y,0) = \mathbf{0}$ for $a \le x \le L/2$ and $a \le y \le L/2$. The mesh used is shown in Fig. 12, where 4×8 elements are placed at the crack surface.

Fig. 13 displays the lower-right of the crack opening displacement profile, at $y = 0$, obtained by the present 3D BEM for four different values of the gradient coefficient g (0.05, 0.1, 0.3, 0.5), as well as the profile corresponding to the classical elastic case ($g = 0$). The profiles are compared to the 2D ones of Fig. 7 and found to be the same as expected. The same conclusion is valid for the calculated $(K_I)_1$ and $(K_I)_2$ SIFs plotted in Figs 14 and 15 for different gradient coefficients g.

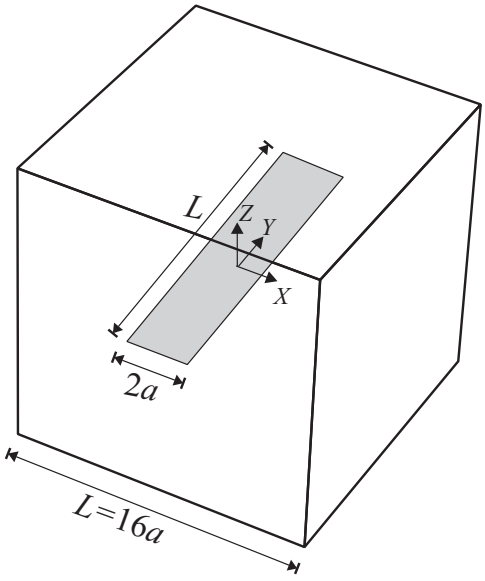

Figure 11: The gradient elastic cube with a central horizontal rectangular crack.

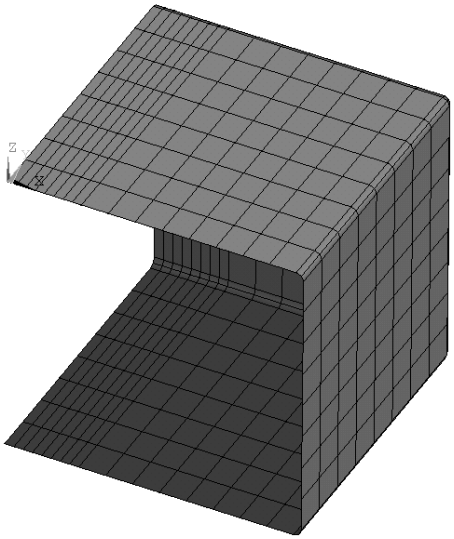

Figure 12: The discretized domain (one eighth of the cube).

6 Conclusions

A displacement based BEM was employed for the solution of 2D and 3D mode-I crack problems characterized by a linear and isotropic gradient elastic material. The Mindlin's simplified

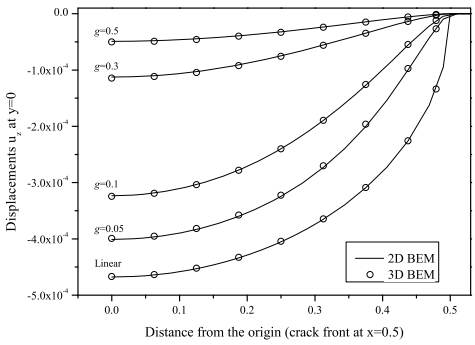

Figure 13: Shape of mode-I crack for different values of the gradient coefficient g.

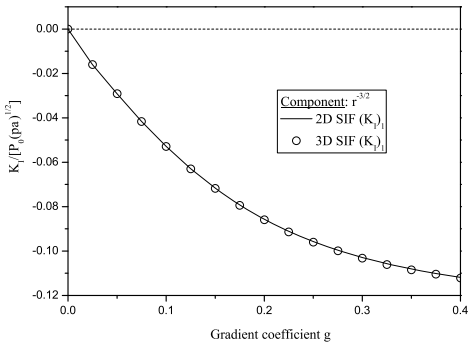

Figure 14: SIF $(K_I)_1$ with respect to the gradient coefficient g.

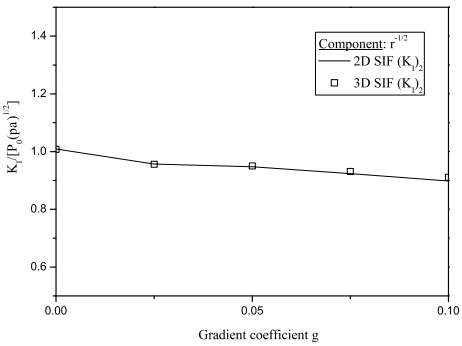

Figure 15: SIF $(K_I)_2$ with respect to the gradient coefficient g.

Form-II gradient elastic theory was adopted and a corresponding 2D and 3D boundary element methodology was employed. A new eight-noded discontinuous boundary element of variable singularity has been developed as an extension to 3D of the corresponding 2D special element proposed by the authors. These special elements can lead to the determination of 2D and 3D SIFs directly via their nodal traction values after the determination of boundary tractions and displacements. Two mode-I crack problems dealing with 2D and 3D cracks were solved for various values of the gradient elastic coefficient. All the results concerning the behavior of the considered fields near the crack tip or front were obtained directly in the context of Mindlin's simplified Form-II gradient elastic theory, without considering extra conditions. Stresses and displacements around the crack tip were calculated with high accuracy and showed to be more physically acceptable than those of the case of classical elasticity.

Acknowledgement: We thank the European Social Fund (ESF), Operational Program for Educational and Vocational Training II (EPEAEK II), and particularly the Greek Program PYTHAGORAS II, for funding the above work.

References

Aifantis, E. C. (1992): On the role of gradients in the localization of deformation and fracture. *International Journal of Engineering Science*, vol. 30, pp. 1279–1299.

Akarapu, S.; Zbib, H. M. (2006): Numerical analysis of plane cracks in strain-gradient elastic materials. *Int. J. Fracture*, vol. 141, pp. 403–430.

Aliabadi, M. H. (1997): Boundary element formulations in fracture mechanics. *Appl. Mech. Rev. ASME*, vol. 50, pp. 83–96.

Amanatidou, E.; Aravas, N. (2002): Mixed finite element formulations of strain-gradient elasticity problems. *Comput. Methods Appl. Mech. Engng.*, vol. 191, pp. 1723–1751.

Amanatidou, E.; Giannakopoulos, A.; Aravas, N. (2005): Finite element models of strain-gradient elasticity: accuracy and error estimates. *G. Georgiou, P. Papanastasiou, M. Papadrakakis (Eds), Proceedings of 5th GRACM International Congress on Computational Mechanics, University of Cyprus, Nicosia*, pp. 797–804.

Askes, H.; Gutierrez, M. A. (2006): Implicit gradient elasticity. *Int. J. Numer. Meth. Engng*, vol. 67, pp. 400–416.

Barenblatt, G. I. (1962): Mathematical theory of equilibrium cracks in brittle fracture. *Adv. Appl. Mech.*, vol. 7, pp. 55–129.

Beskos, D. E. (1997): Boundary element methods in dynamic analysis. Part II (1986-1996). *Appl. Mech. Rev. ASME*, vol. 50, pp. 149–197.

Casal, P. (1972): La theorie du second gradient et la capillarite. *C.R. Acad. Sc.*, vol. A247, pp. 1571–1574.

Dessouky, S.; Masad, E.; Little, D.; Zbib, H. (2006): Finite-Element Analysis of Hot Mix Asphalt Microstructure Using Effective Local Material Properties and Strain Gradient Elasticity. *Journal of Engineering Mechanics*, pp. 158–171.

Dessouky, S.; Masad, E.; Zbib, H.; Little, D. (2003): Gradient elasticity finite element model for the microstructure analysis of asphaltic materials. *K.J. Bathe (Ed.), Computational Fluid and Solid Mechanics, Elsevier, London*, pp. 228–233.

Dominguez, J.; Ariza, M. P. (2003): Hypersingular and mixed boundary elements in fracture mechanics. *D. Beskos, G. Maier (Eds), Boundary Element Advances in Solid Mechanics, Springer, Wien*, pp. 115–165.

Engel, G.; Garikipati, K.; Hughes, T. J. R.; Larson, M. G.; Mazzei, L.; Taylor, R. L. (2002): Continuous/discontinuous finite element approximations of fourth-order elliptic problems in structural and continuum mechanics with applications to thin beams and plates, and strain gradient elasticity. *Comput. Methods Appl. Mech. Engrg.*, vol. 191, pp. 3669–3750.

Exadaktylos, G. E. (1998): Gradient elasticity with surface energy: mode-I crack problem. *Int. J. Solids Struct.*, vol. 35, pp. 421–456.

Exadaktylos, G. E.; Vardoulakis, I. (1998): Surface instability in gradient elasticity with surface energy. *Int. J. Solids Structures*, vol. 35, pp. 2251–2281.

Exadaktylos, G. E.; Vardoulakis, I. (2001): Microstructure in linear elasticity and scale effects: a reconsideration of basic rock mechanics and rock fracture mechanics. *Tectonophysics*, vol. 335, pp. 81–109.

Exadaktylos, G. E.; Vardoulakis, I.; Aifantis, E. (1996): Cracks in gradient elastic bodies with surface energy. *Int. J. Fract.*, vol. 79, pp. 107–119.

Fannjiang, A. C.; Chan, Y. S.; Paulino, G. H. (2002): Strain gradient elasticity for antiplane shear cracks: a hypersingular integrodifferential equation approach. *SIAM J. Appl. Math.*, vol. 62, pp. 1066–1091.

Fleck, N. A.; Hutchinson, J. W. (1997): Strain gradient plasticity. *Hutchinson, J.W., Wu, T.Y. (Eds.), Advances in Applied Mechanics, Academic Press, New York*, vol. 33, pp. 295–361.

Fleck, N. A.; Hutchinson, J. W. (2001): A reformulation of strain gradient plasticity. *J.Mech.Phys.Solids*, vol. 49, pp. 2245–2271.

Fujimoto, T.; Nishioka, T. (2006): Numerical Simulation of Dynamic Elasto Visco-plastic Fracture Using Moving Finite Element Method. *CMES:Computer Modeling in Engineering & Sciences*, vol. 11, pp. 91–102.

Georgiadis, H. G. (2003): The mode III crack problem in microstructured solids governed by dipolar gradient elasticity: static and dynamic analysis. *J. Appl. Mech. ASME*, vol. 70, pp. 517–530.

Georgiadis, H. G.; Grentzelou, C. G. (2006): Energy theorems and the J-integral in dipolar gradient elasticity. *Int. J. Solids Struct*, vol. 43, pp. 5690–5712.

Green, A. E.; Rivlin, R. S. (1964): Multipolar Continuum Mechanics. *Arch. Ration. Mech. Anal.*, vol. 17, pp. 113–147.

Guiggiani, M.; Gigante, A. (1990): A general algorithm for multidimensional Cauchy principal value integrals in the boundary element method. *J. Appl. Mech. ASME*, vol. 57, pp. 906–915.

Huang, Y.; Zhang, L.; Guo, T. F.; Hwang, K. C. (1997): Mixed mode near-tip fields for cracks in materials with strain-gradient effects. *J. Mech. Phys. Solids*, vol. 45, pp. 439–465.

Imatani, S.; Hataday, K.; Maugin, G. A. (2005): Finite element analysis of crack problems for strain gradient material model. *Philosophical Magazine*, vol. 85, pp. 4245–4256.

Karlis, G. F.; Tsinopoulos, S. V.; Polyzos, D.; Beskos, D. E. (2007): Boundary element analysis of mode I and mixed mode (I and II) crack problems of 2-D gradient elasticity. *Comput. Methods Appl. Mech. Engrg.*, vol. 196, pp. 5092–5103.

Lim, K. M.; Lee, K. H.; Tay, A. A. O.; Zhou, W. (2002): A new variable-order singular boundary element for two-dimensional stress analysis. *Int. J. Numer. Meth. Engng.*, vol. 55, pp. 293–316.

Markolefas, S. I.; Tsouvalas, D. A.; Tsamasphyros, G. I. (2007): Theoretical analysis of a class of mixed, C^0 continuity formulations for general dipolar gradient elasticity boundary value problems. *Int. J. Solids Struct.*, vol. 44, pp. 546–572.

Mindlin, R. D. (1964): Micro-structure in linear elasticity. *Arch. Rat. Mech. Anal.*, vol. 16, pp. 51–78.

Mindlin, R. D. (1965): Second gradient of strain and surface-tension in linear elasticity. *International Journal of Solids and Structures*, vol. 1, pp. 417–438.

Mindlin, R. D.; Eshel, N. N. (1968): On first strain-gradient theories in linear elasticity. *Int. J. Solids Struct.*, vol. 4, pp. 109–124.

Nishioka, T.; Kabayashi, Y.; Fujimoto, T. (2007): The Moving Finite Element Method Based on Dalaunay Automatic Triangulation For

Fracture Path Prediction Simulations In Nonlinear Elastic-Plastic Materials. *CMES:Computer Modeling in Engineering & Sciences*, vol. 17, pp. 231–238.

Peerlings, R. H. J.; Fleck, N. A. (2004): Computational Evaluation of Strain Gradient Elasticity Constants. *International Journal for Multiscale Computational Engineering*, vol. 2, pp. 599–619.

Polyzos, D. (2005): 3D Frequency domain BEM for solving dipolar gradient elastic problems. *Comput. Mech.*, vol. 35, pp. 292–304.

Polyzos, D.; Tsepoura, K. G.; Beskos, D. E. (2005): Transient dynamic analysis of 3-D gradient elastic solids by BEM. *Comput. Struct.*, vol. 83, pp. 783–792.

Polyzos, D.; Tsepoura, K. G.; Tsinopoulos, S. V.; Beskos, D. E. (2003): A boundary element method for solving 2-D and 3-D static gradient elastic problems. Part I: Integral formulation. *Comput. Meth. Appl. Mech. Engng*, vol. 192, pp. 2845–2873.

Radi, E. (2008): On the effects of characteristic lengths in bending and torsion on mode III crack in couple stress elasticity. *Int. J. Solids Struct.* to appear.

Ru, C. Q.; Aifantis, E. C. (1993): A simple approach to solve boundary value problems in gradient elasticity. *Acta Mechanica*, vol. 101, pp. 59–68.

Shah, P. D.; Tan, C. L.; Wang, X. (2006): Evaluation of T-stress for An Interface Crack between Dissimilar Anisotropic Materials Using the Boundary Element Method. *CMES:Computer Modeling in Engineering & Sciences*, vol. 13, pp. 185–198.

Shi, M. X.; Huang, Y.; Hwang, K. C. (2000): Fracture in a higher-order elastic continuum. *J. Mech. Phys. Solids*, vol. 48, pp. 2513–2538.

Shu, J. Y.; King, W. E.; Fleck, N. A. (1999): Finite elements for materials with strain gradient effects. *Int. J. Numer. Meth. Engng.*, vol. 44, pp. 373–391.

Soh, A. K.; Wanji, C. (2004): Finite element formulations of strain gradient theory for microstructures and the C0-1 patch test. *Int. J. Numer. Meth. Engng.*, vol. 61, pp. 433–454.

Tang, Z.; Shen, S.; Atluri, S. N. (2003): Analysis of materials with strain-gradient effects: A meshless local Petrov-Galerkin (MLPG) approach, with nodal displacements only. *CMES:Computer Modeling in Engineering & Sciences*, vol. 4, pp. 177–196.

Tenek, L. T.; Aifantis, E. C. (2002): A two-dimensional finite element implementation of a special form of gradient elasticity. *CMES:Computer Modeling in Engineering & Sciences*, vol. 3, pp. 731–741.

Tong, P.; Lam, D. C. C.; Yang, F. (2005): Mode I solution for micron-sized crack. *Engineering Fracture Mechanics*, vol. 72, pp. 1779–1804.

Tsepoura, K. G.; Papargyri-Beskou, S.; Polyzos, D. (2002): A boundary element method for solving 3-D static gradient elastic problems with surface energy. *Comput. Mech.*, vol. 29, pp. 361–381.

Tsepoura, K. G.; Polyzos, D. (2003): Static and harmonic BEM solutions of gradient elasticity problems with axisymmetry. *Comput. Mech.*, vol. 32, pp. 89–103.

Tsepoura, K. G.; Tsinopoulos, S.; Polyzos, D.; Beskos, D. E. (2003): A boundary element method for solving 2-D and 3-D static gradient elastic problems. Part II: Numerical implementation. *Comput. Meth. Appl. Mech. Engng.*, vol. 192, pp. 2875–2907.

Vardoulakis, I.; Exadaktylos, G. (1997): The asymptotic solution of anisotropic gradient elasticity with surface energy for mode-II crack. *D. Durban (Ed.), Non-linear Singularities in Deformation and Flow, Kluwer Academic Publishers, Dordrecht*, pp. 87–98.

Vardoulakis, I.; Exadaktylos, G. E.; Aifantis, E. D. (1996): Gradient elasticity with surface energy: mode-III crack problem. *Int. J. Solids Struct.*, vol. 33, pp. 4531–4559.

Vardoulakis, I.; Giannakopoulos, A. E. (2006): An example of double forces taken from structural analysis. *Int. J. Solids Struct.*, vol. 43, pp. 4047–4062.

Vardoulakis, I.; Sulem, J. (1995): *Bifurcation Analysis in Geomechanics*. Chapman and Hall, London.

Wei, Y. (2006): A new finite element method for strain gradient theories and application to fracture analyses. *European J. Mech. A/Solids*, vol. 25, pp. 897–913.

Wen, P. H.; Aliabadi, M. H.; Young, A. (2002): Boundary Element Analysis of Curved Cracked Panels with Mechanically Fastened Repair Patches. *CMES:Computer Modeling in Engineering & Sciences*, vol. 3, pp. 1–10.

Zhang, C.; Savaidis, A. (2003): 3-D Transient Dynamic Crack Analysis by a Novel Time-Domain BEM. *CMES:Computer Modeling in Engineering & Sciences*, vol. 4, pp. 603–.

Zhang, L.; Huang, Y.; Chen, J. Y.; Hwang, K. C. (1998): The mode III full-field solutions in elastic materials with strain gradient effects. *Int. J. Fracture*, vol. 92, pp. 325–348.

Zhou, W.; Lim, K. M.; Lee, K. H.; Tay, A. A. (2005): A new variable-order singular boundary element for calculating stress intensity factors in three-dimensional elasticity problems. *Int. J. Solids Struct.*, vol. 42, pp. 159–185.

Appendix A: 3D Integrations over the Special Elements

In this section, the treatment of the integrals appearing in Eqs (39) and (40) for the 3D case is explained. The integrals involving the fields **P** and **R** and defined over the special boundary elements, in addition to the usual fundamental solution type of singularities (Tsepoura, Tsinopoulos, Polyzos, and Beskos (2003)), exhibit an extra singularity due to the singular behavior of the interpolation functions near the crack front. Thus, even in cases where the source point does not reside in the element, i.e., in cases where a so-called regular integration is performed, there is always a singularity present near the front of the crack. The methodology for the treatment of these integrals deals first with the handling of the singularities coming from the interpolation functions of the special element and then addresses any possible singularities that are introduced by the fundamental solutions (in case the source point resides in the element). Without loss of generality, one can assume that the crack front resides at the first side of the element. If it does not, one can renumber the element nodes so that it does. This assumption is useful for the simplification of the following paragraphs.

Appendix A:.1 Integrals involving the field **R**

The integrals involving the field **R** and are defined over a special boundary element, appear in the discretized form of Eqs (39) and (40) as

$$\int_{-1}^{1}\int_{-1}^{1} \frac{\partial \tilde{\mathbf{u}}^*}{\partial n_y}(\mathbf{x}(\xi_1,\xi_2),\mathbf{y}) \; N_i(\xi_1, r(\xi_1,\xi_2);\lambda_1,\lambda_2) J_e d\xi_1 d\xi_2$$
$$\int_{-1}^{1}\int_{-1}^{1} \frac{\partial^2 \tilde{\mathbf{u}}^*}{\partial n_x \partial n_y}(\mathbf{x}(\xi_1,\xi_2),\mathbf{y}) \; N_i(\xi_1, r(\xi_1,\xi_2);\lambda_1,\lambda_2) J_e d\xi_1 d\xi_2 \tag{45}$$

where N_i is the ith interpolation function given by Eqs (31), with the parameters λ_1 and λ_2 being equal to $-1/2$ and 1, respectively (Tab. 1) and J_e is the Jacobian of the transformation from the global coordinates to the intrinsic local coordinates ξ_1, ξ_2. It is important to see that there is a singularity of the form $r^{-1/2}$, attributed to the new interpolation functions (31). If r is expanded in series with respect to ξ_2, around the singular point $\xi_2 = -1$ it is easy to see that r is of the following form:

$$r = f(\xi_1)(\xi_2+1)^{-1/2} + \mathrm{O}(\xi_2+1)^{1/2} \tag{46}$$

In order to deal with this new singularity, one applies the nonlinear transformation

$$s_1 = \xi_1$$
$$s_2 = 2\left(\frac{1+\xi_2}{2}\right)^a - 1 \tag{47}$$

which was introduced by Zhou, Lim, Lee, and Tay (2005) and the integrals (45) become

$$\int_{-1}^{1}\int_{-1}^{1} \frac{\partial \tilde{\mathbf{u}}^*}{\partial n_y}(\mathbf{x}(s_1,s_2),\mathbf{y}) N_i(s_1,r(s_1,s_2);\lambda_1,\lambda_2) J_e J_{nl} ds_1 ds_2$$
$$\int_{-1}^{1}\int_{-1}^{1} \frac{\partial^2 \tilde{\mathbf{u}}^*}{\partial n_x \partial n_y}(\mathbf{x}(s_1,s_2),\mathbf{y}) N_i(s_1,r(s_1,s_2);\lambda_1,\lambda_2) J_e J_{nl} ds_1 ds_2 \quad (48)$$

where J_{nl} is the Jacobian of the non-linear transformation (47) of the form

$$J_{nl} = \frac{1}{a}\left(\frac{1+s_2}{2}\right)^{(1-a)/a} \quad (49)$$

and the parameter $a > 0$ is a constant to be determined. For $0 < a \leq 1/2$, the transformation completely removes the interpolation function singularity. In the present work the value $a = 1/2$ is used. As long as the singular behavior of the interpolation functions has been overcome, integrals (48) are treated in the same way as the integrals corresponding to non-special elements (Tsepoura, Tsinopoulos, Polyzos, and Beskos (2003)).

Appendix A:.2 Integrals involving the field **P**

The integrals involving the field **P** and defined over a special boundary element, appear in the discretized form of Eqs (39) and (40) as

$$\int_{-1}^{1}\int_{-1}^{1} \tilde{\mathbf{u}}^*(\mathbf{x}(\xi_1,\xi_2),\mathbf{y}) N_i(\xi_1,r(\xi_1,\xi_2);\lambda_1,\lambda_2) J_e d\xi_1 d\xi_2$$

$$\int_{-1}^{1}\int_{-1}^{1} \frac{\partial \tilde{\mathbf{u}}^*}{\partial n_x}(\mathbf{x}(\xi_1,\xi_2),\mathbf{y}) N_i(\xi_1,r(\xi_1,\xi_2);\lambda_1,\lambda_2) J_e d\xi_1 d\xi_2 \quad (50)$$

where the parameters λ_1 and λ_2 are equal to $-3/2$ and $-1/2$, respectively (Tab. 1). This time to deal with the interpolation function singularities, the aforementioned nonlinear transformation is not adequate. Since the singularities introduced by the interpolation functions are more than one (of the orders of $r^{-3/2}$ and $r^{-1/2}$), the nonlinear transformation raises their order only partially. Again, expanding $r^{-3/2}$ in series around the singular point $\xi_2 = -1$, one can see that r is given by

$$r = f(\xi_1)(\xi_2+1)^{-3/2} + g(\xi_1)(\xi_2+1)^{-1/2} + \mathrm{O}(\xi_2+1)^{1/2} \quad (51)$$

After applying the nonlinear transformation (47) the integrals (50) become

$$\int_{-1}^{1}\int_{-1}^{1} \tilde{\mathbf{u}}^*(\mathbf{x}(s_1,s_2),\mathbf{y}) N_i(s_1,r(s_1,s_2);\lambda_1,\lambda_2) J_e J_{nl} ds_1 ds_2$$

$$\int_{-1}^{1}\int_{-1}^{1} \frac{\partial \tilde{\mathbf{u}}^*}{\partial n_x}(\mathbf{x}(s_1,s_2),\mathbf{y}) N_i(\xi_1,r(s_1,s_2);\lambda_1,\lambda_2) J_e J_{nl} ds_1 ds_2 \quad (52)$$

Observing the transformation, one can notice that there is no value for the parameter a that raises the order of both interpolation function singularities. However, by choosing $a = 1/2$ one can reduce the singularities to the order of r^{-1}. To address this type of singularity one also applies the methodology for direct treatment of singular integrals, introduced by Guiggiani and Gigante (1990). In short, the kernels of the integrals are expanded asymptotically to power series with respect to the local coordinate s_2 around the point $s_2 = -1$. Then the singular terms of the divergent part of the integrals are subtracted and the integral is calculated with the Gauss quadrature, as it is now regular and finally the subtracted terms are added, after integrating them analytically. Applying the above briefly described procedure, the

integrals (52) take the form

$$\int_{-1}^{1}\left[\int_{-1}^{1}\tilde{\mathbf{u}}^{*}N_i\left(s_1,r\left(s_1,s_2\right);\lambda_1,\lambda_2\right)\left(\frac{1+s_2}{2}\right)\right.$$
$$J_e\left(s_1,s_2\right)-\tilde{\mathbf{u}}^{*}|_{s_2=-1}A\,J_e|_{s_2=-1}\left(\frac{1+s_2}{2}\right)^{-2}ds_2$$
$$\left.+\tilde{\mathbf{u}}^{*}|_{s_2=-1}A\,J_e|_{s_2=-1}\lim_{\varepsilon\to 0}\int_{-1+\varepsilon}^{1}\left(\frac{1+s_2}{2}\right)^{-2}ds_2\right]$$
$$ds_1 \quad (53)$$

$$\int_{-1}^{1}\left[\int_{-1}^{1}\frac{\partial\tilde{\mathbf{u}}^{*}}{\partial n_x}N_i\left(s_1,r\left(s_1,s_2\right);\lambda_1,\lambda_2\right)\left(\frac{1+s_2}{2}\right)\right.$$
$$J_e\left(s_1,s_2\right)$$
$$-\left.\frac{\partial\tilde{\mathbf{u}}^{*}}{\partial n_x}\right|_{s_2=-1}A\,J_e|_{s_2=-1}\left(\frac{1+s_2}{2}\right)^{-2}ds_2$$
$$+\left.\frac{\partial\tilde{\mathbf{u}}^{*}}{\partial n_x}\right|_{s_2=-1}A\,J_e|_{s_2=-1}$$
$$\left.\lim_{\varepsilon\to 0}\int_{-1+\varepsilon}^{1}\left(\frac{1+s_2}{2}\right)^{-2}ds_2\right]ds_1 \quad (54)$$

where ε is the radius of a sphere including the singular point, which resides on the crack front. The analytical calculation of the last integrals appearing in Eqs (54), (55) yields

$$\lim_{\varepsilon\to 0}\int_{-1+\varepsilon}^{1}\left(\frac{1+s_2}{2}\right)^{-2}ds_2=\lim_{\varepsilon\to 0}\left(-\frac{4}{1+s_2}\Big|_{-1+\varepsilon}^{1}\right)$$
$$=-2+\lim_{\varepsilon\to 0}\frac{4}{\varepsilon} \quad (55)$$

Considering the contribution of all elements around the singular point within a neighbourhood of size ε, the last term in Eq. (55) must be zero (Guiggiani and Gigante (1990)). As long as the singular behavior of the interpolation functions has been overcome, the integrals (54) are treated in the same way as the integrals corresponding to non-special elements (Tsepoura, Tsinopoulos, Polyzos, and Beskos (2003)).

Appendix A:.3 Integrals involving the field $\mathbf{q}$

The integrals involving the field $\mathbf{q}$ and defined over a special boundary element, appear in the discretized form of Eqs (39) and (40) as

$$\int_{-1}^{1}\int_{-1}^{1}\tilde{\mathbf{R}}^{*}\left(\mathbf{x}\left(\xi_1,\xi_2\right),\mathbf{y}\right)N^{i}\left(\xi_1,r\left(\xi_1,\xi_2\right);\lambda_1,\lambda_2\right)$$
$$J_e d\xi_1 d\xi_2$$

$$\int_{-1}^{1}\int_{-1}^{1}\frac{\partial\tilde{\mathbf{R}}^{*}}{\partial n_x}\left(\mathbf{x}\left(\xi_1,\xi_2\right),\mathbf{y}\right)N^{i}\left(\xi_1,r\left(\xi_1,\xi_2\right);\lambda_1,\lambda_2\right)$$
$$J_e d\xi_1 d\xi_2 \quad (56)$$

where the parameters λ_1 and λ_2 are equal to $1/2$ and 1, respectively (Tab. 1). The interpolation functions involved in integrals (56) do not exhibit any singularity as one approaches the crack front. Thus, one would expect that a standard Gauss quadrature would be adequate for an accurate integration. However, a slow convergence was observed due to the $O\left(r^{1/2}\right)$ term of the interpolation functions. In order to achieve a better convergence, the non-linear transformation (47) is used again with $a=1/2$, this time in an effort to increase the order of the integrand from $O\left(r^{1/2}\right)$ to $O\left(r^{3/2}\right)$. Thus the integrals (56) finally become

$$\int_{-1}^{1}\int_{-1}^{1}\tilde{\mathbf{R}}^{*}\left(\mathbf{x}\left(s_1,s_2\right),\mathbf{y}\right)N_i\left(s_1,r\left(s_1,s_2\right);\lambda_1,\lambda_2\right)$$
$$J_e J_{nl} ds_1 ds_2$$

$$\int_{-1}^{1}\int_{-1}^{1}\frac{\partial\tilde{\mathbf{R}}^{*}}{\partial n_x}\left(\mathbf{x}\left(s_1,s_2\right),\mathbf{y}\right)N_i\left(s_1,r\left(s_1,s_2\right);\lambda_1,\lambda_2\right)$$
$$J_e J_{nl} ds_1 ds_2 \quad (57)$$

where J_{nl} is the Jacobian of the non-linear transformation given by (49).